CHANGES IN THE INTERLAYER STRUCTURE AND THERMODYNAMICS OF HYDRATED MONTMORILLONITE UNDER BASIN CONDITIONS: MOLECULAR SIMULATION APPROACHES

Jinhong Zhou[1], Xiancai Lu[1,]*, and Edo S. Boek[2]

[1] State Key Laboratory for Mineral Deposits Research, School of Earth Sciences and Engineering, Nanjing University, Nanjing 210023, China
[2] Department of Chemistry, University of Cambridge, Lensfield Road, CB2 1EW, Cambridge, UK

Abstract—Interlayer swelling of hydrated montmorillonite is an important issue in clay mineralogy. Although the swelling behavior of montmorillonite under ambient conditions has been investigated comprehensively, the effects of basin conditions on the hydration and swelling behaviors of montmorillonite have not been characterized thoroughly. In the present study, molecular dynamics simulations were employed to reveal the swelling behavior and changes in the interlayer structure of Na-montmorillonite under the high temperatures and pressures of basin conditions. According to the calculation of the immersion energy, the monolayer hydrate becomes more stable than the bilayer hydrate at a burial depth of 7 km (at a temperature of 518 K and a lithostatic pressure of 1.04 kbar). With increasing burial depth, the basal spacings of the monolayer and bilayer hydrates change to varying degrees. The density-distribution profiles of interlayer species exhibit variation in the hydrate structures due to temperature and pressure change, especially in the structures of bilayer hydrate. With increasing depth, more Na^+ ions prefer to distribute closer to the clay layers. The mobility of interlayer water and ions increases with increasing temperature, while increasing pressure caused the mobility of these ions to decrease.

Key Words—Basin Conditions, Hydration, Molecular Dynamics Simulation, Montmorillonite, Swelling.

INTRODUCTION

The swelling of clay minerals, especially mont-morillonite, has attracted considerable attention in recent decades due to the importance of hydration states and interlayer structure in developing materials for industrial applications and understanding hydrogeological and geological processes (Cases *et al.*, 1992; Berend *et al.*, 1995; Boek *et al.*, 1995a, 1995b; De Siqueira *et al.*, 1999; Deming, 2002; Liu and Lu, 2006). In general, naturally occurring hydration and dehydration of swel-ling clays in petroleum-bearing basins greatly affect the stability of the clay-enriched formations and further influence oil-drilling operations and water-flooding efficiency, which occasionally increases well-construc-tion costs and decreases petroleum-recovery perfor-mance (Anderson *et al.*, 2010). Clay swelling also plays a critical role in the subsurface migration of geofluids, petroleum, and contaminants (De Siqueira *et al.*, 1999; Hensen and Smit, 2002; Anderson *et al.*, 2010).

The intracrystalline hydration and dehydration of montmorillonite under ambient conditions has been investigated experimentally and theoretically for a broad range of applications (Laird, 1999; Xu *et al.*,

2000; Boek and Sprik, 2003; Ferrage *et al.*, 2005a, 2005b, 2010). In previous studies, the monolayer and bilayer hydrates were both well defined in experiments and simulations, while the formation of three-layer hydrates in montmorillonite under ambient conditions has been recorded in more recent studies (Holmboe *et al.*, 2012; Dazas *et al.*, 2014; Holmboe and Bourg, 2014; Teich-McGoldrick *et al.*, 2015). Multiple experimental methods have been used to study clay swelling, including *in situ* X-ray diffraction (XRD) (Brown and Brindley, 1980), Fourier-transform infrared (FTIR) spectroscopy (Petit and Madejová, 2013), and thermo-gravimetric analysis (TGA) (Guggenheim and Van Groos, 2001), among others. Experimental studies of the intracrystalline hydration/dehydration of mont-morillonite with various interlayer cations were carried out by Cases and colleagues (Cases *et al.*, 1992, 1997; Berend *et al.*, 1995). In the previous decade, molecular simulation appeared to be a complementary tool to the existing experimental methods, not only providing reliable information about thermodynamics of clay swelling, but also a detailed atomic/molecular-scale description of the interlayer structures. Since the development of simulation techniques and new force fields (Teppen *et al.*, 1997; Cygan *et al.*, 2004; Heinz *et al.*, 2005), the studies of interlayer structures to acquire information about the dynamics of hydrated mont-morillonite and its swelling mechanisms have been performed extensively (De Siqueira *et al.*, 1997; Smith,

1998; Hensen and Smit, 2002; Smith *et al.*, 2006; Wang *et al.*, 2006; Cygan *et al.*, 2009; Teich-McGoldrick *et al.*, 2015).

In the last decade, the effects of geological conditions on the hydration and swelling of clays has become an area of significant interest (Odriozola and Guevara-Rodríguez, 2004; Shahriyari *et al.*, 2013; Holmboe and Bourg, 2014). Time-of-flight neutron diffraction experiments were employed by De Siqueira *et al.* (1999) to study the influence of high temperatures and pressures on the swelling of vermiculite and smectite as well as their transition temperatures. Those authors found that the change from trilayer hydrate to bilayer hydrate occurs at a temperature of 633 K and a pressure of 1.8 kbar (corresponding to a depth of ~12 km). The transition temperatures and pressures from a bilayer to a monolayer of montmorillonite were observed at values of 798 K and 5±1.4 kbar (Huang *et al.*, 1994; Wu *et al.*, 1997). The grand canonical ensemble (μVT) was used by De Pablo *et al.* (2005) to study the swelling of montmorillonite under borehole conditions and those authors proposed different transition points for Na-montmorillonite with increasing depth: one-layer hydrates that are stable at temperatures between 333 and 533 K and pressures between 0.30 and 1.30 kbar, and two- or three-layer hydrates occurring at a temperature of ~533 K and a pressure of ~1.30 kbar. This finding means that, in sedimentary basins, the two-layer hydrate of Na-montmorillonite is located at an approximate depth of 8.7 km, while the one-layer hydrates will be the stable phase above this depth (De Pablo *et al.*, 2005). The stable hydration states under borehole conditions, as well as the temperatures and pressures of their transitions points, are still under debate.

A molecular dynamics (MD) simulation study was carried out to understand the swelling behaviors of Na-montmorillonite under borehole conditions. The influences of the temperature and pressure on the swelling behaviors were ascertained from detailed comparisons of swelling curves, density-distribution profiles, and diffusion coefficients.

METHODOLOGY

Clay model

In this study the clay used was Wyoming-type montmorillonite (Wyo) which has a unit-cell formula of $Na_{0.75}(Si_{7.75}Al_{0.25})(Al_{3.5}Mg_{0.5})O_{20}(OH)_4$. The CEC of the model is equal to 102 meq/100 g of clay (Boek *et al.*, 1995b), the layer charge is 0.75 e per unit cell, with tetrahedral substitutions (Al for Si) and octahedral substitutions (Mg for Al) that obey Loewenstein's rule (*i.e.* two substitution sites cannot be adjacent) (Loewenstein, 1954). The clay model used in the present simulations consists of two clay TOT layers of 16 unit cells obtained after replication of the initial unit cell by

factors of $(4 \times 2 \times 2)$ along the *a*, *b*, and *c* crystallographic directions, respectively. The initial basal spacing of montmorillonite is ~10 Å and periodic boundary conditions were imposed on all of the simulated systems present.

Simulation details

All MD simulations were undertaken using the *LAMMPS* package (Plimpton, 1995). The well known SPC (simple point charge) model (Rick *et al.*, 1994) was used to describe water–molecule interactions while the clay atoms were treated using the *CLAYFF* force field (Cygan *et al.*, 2004) which has been used extensively in previous simulation studies of clays and other related minerals (Wang *et al.*, 2004; Greathouse *et al.*, 2005; Kim *et al.*, 2005; Liu and Lu, 2006; Liu *et al.*, 2008; Cygan *et al.*, 2009; Zhang *et al.*, 2014).

Montmorillonite is found in argillaceous or clay-bearing rocks at depths even greater than 10 km (Meunier, 2005). Three depths (3.0, 5.0, and 7.0 km) were investigated in the present study, therefore, and the corresponding temperatures and pressures are listed in Table 1. Ambient conditions (298 K, 1.0 bar) were employed as a reference system. Both hydrostatic pressure (NP) and lithostatic pressure (SP) were considered. The lithostatic pressure, which commonly occurs in basins (especially with overpressure when the depth is >3.0 km), was calculated with the weight of the entire overburden (Deming, 2002). The temperature and pressure values given in Table 1 for different depths were evaluated using the following equations:

$$T = T_0 + T_{gradient} \quad (1)$$

$$NP = NP_0 + NP_{gradient} \quad (2)$$

$$SP = 1.5 \times NP \quad (3)$$

In equations 1−3, *T*, *NP*, and *SP* are the working temperature, hydrostatic pressure, and lithostatic pressure, respectively, used in the present study; $T_0 = 14ºC$ and $NP_0 = 1$ bar are the average values of the temperature and hydrostatic pressure at the soil surface in eastern China; and $T_{gradient}$ and $NP_{gradient}$ are the temperature and hydrostatic pressure gradients. The

Table 1. Temperature and pressure at different depths considered in this study.

Depth (km)	Temperature (K)	NP (kbar)	SP (kbar)
0 (Ambient)	298.15	0.001	—
3.0	386	0.30	—
5.0	452	0.50	0.74
7.0	518	0.69	1.04

NP: hydrostatic fluid pressure; SP: lithostatic pressure.

temperature gradient was assumed to be 33ºC km^{-1}, which is analogous to the petroleum-bearing depressions in eastern China (Zhang *et al.*, 2014). The hydrostatic fluid-pressure gradient was assumed to be 98 bar km^{-1}, and the lithostatic pressure was determined using a formation overpressure coefficient of 1.5 as the depth was >3.0 km (Hunt, 1990; Xie *et al.*, 2001).

To determine the swelling curves and immersion energies of Na-montmorillonite under basin conditions, 16 NPT-ensemble MD simulations with a wide range of interlayer water contents (from 0 to 388 mg/g) were performed for each of the depth values in Table 1. In the initial configurations, water molecules and interlayer ions were placed randomly in the interlayer spaces. Each of the NPT simulations was run for 2.0 ns to reach an equilibrium state prior to a 1.0 ns production run. In these NPT simulations, the volume changes of the simulation cell were only allowed in the *z* direction. The equilibrium basal spacings of Na-montmorillonite and the potential energies of the systems were calculated from the 1.0 ns production run and the immersion energy curves were deduced from these potential energies (Boek *et al.*, 1995b; Smith, 1998; Liu and Lu, 2006; Kumar *et al.*, 2007; Liu *et al.*, 2008).

In the swelling and immersion energy curves two stable hydrates were identified and (their simulation systems) were employed to study the structural and dynamical behavior of the hydrated Na-montmorillonite at different depths. This was achieved through NVT-ensemble MD simulations for 1.0 ns with the starting point being the last configuration of the previous 3.0 ns NPT simulations. In all the simulations carried out in the present study, a timestep of 1.0 fs was used with a frequency of 100 fs for recording trajectories. The cut-off for short-range interaction was set as 9.0 Å and Ewald summations were used for the Coulombic interactions. The number of *k*-space vectors was determined to reach a precision of 1×10^{-4} with the pairwise calculation within a cut-off of 9.0 Å.

Simulation analyses

The basal spacings (*Z*) were calculated from the following equation:

$$Z = <V>/(S \times 2) \qquad (4)$$

Where $<V>$ is the box volume averaged over the 1.0 ns production run in the NPT-ensemble and $S = a \times b$ is the basal surface area.

Immersion energy was used to describe the swelling thermodynamics of montmorillonite. The immersion energy *Q* was calculated as

$$Q = <U(N)> - <U(N^0)> - (N - N^0)U_{bulk} \qquad (5)$$

Where $<U(N)>$ is the averaged potential energy (over the last 1.0 ns of NPT-ensemble simulations) of the montmorillonite with water content *N*, U_{bulk} stands for the internal energy of bulk water, and N^0 is the water

content of the selected reference state that has the greatest water content in the present study.

The atomic-density distribution profiles along the *z* direction of clay minerals were calculated by averaging the trajectories from the NVT simulations and were used to describe the organization of the interlayer species along that direction. The surfaces of clay layers in the box edge were used as the origin (*z* = 0). The atomic density is defined as:

$$\rho(z) = <N(z - \Delta z/2, z + \Delta z/2)>/(\Delta z \times S) \qquad (6)$$

In this equation $<N(z - \Delta z/2, z + \Delta z/2)>$ is the average number of atoms distributed among the area in the height interval of $(z - \Delta z/2, z + \Delta z/2)$. Δz was set at 0.5 Å.

The self-diffusion coefficients (*D*) of the interlayer species were calculated by the Einstein relation:

$$\frac{1}{N}\sum_{i=1}^{N}\langle|r_i(t) - r_i(0)|^2\rangle = 2dDt \qquad (7)$$

In this equation, *N* is the number of atoms of a given species in the simulation cell, $r_i(t)$ is the center-of-mass position of the *i*th atom at time *t*, and *d* is the diffusion dimensionality. The left part of equation 7 is defined as the mean squared displacement (MSD).

RESULTS

Swelling curves

The swelling curves of Na-montmorillonite at various depths are shown in Figure 1. As expected, the basal spacings increase with increasing water content. The basal spacings also increase with increasing depths when the water content is >150 mg/g of clay, which is caused by the combined effects of temperature and pressure. Two plateaus can be identified on the swelling curves indicating the formation of monolayer hydrates (the first plateau in Figure 1, between 60 and 135 mg/g of clay) and bilayer hydrates (the second plateau in Figure 1, between 180 and 235 mg/g of clay). The swelling curve of ambient conditions is consistent with the previous studies (Boek *et al.*, 1995a; Tambach *et al.*, 2004). Under both NP and SP the basal spacings of monolayer hydrates at different depths are all located around 12 Å (Figure 1) and increasing the temperature and pressure has just a minor effect on these values. This effect is more pronounced for the bilayer hydrates which were shown in the dotted square (in the part of the figure on the right) between 180 and 235 mg/g of clay (Figure 1). The basal spacing at greater depth was consistently slightly larger than it was at shallower depths under both NP and SP states. In theory the local minima of immersion energy curves indicate stable hydrate states while the global minimum indicates the most stable hydration state. The first minimum of the immersion energy curve of montmorillonite indicates the monolayer hydrate while the second points out the bilayer hydrate.
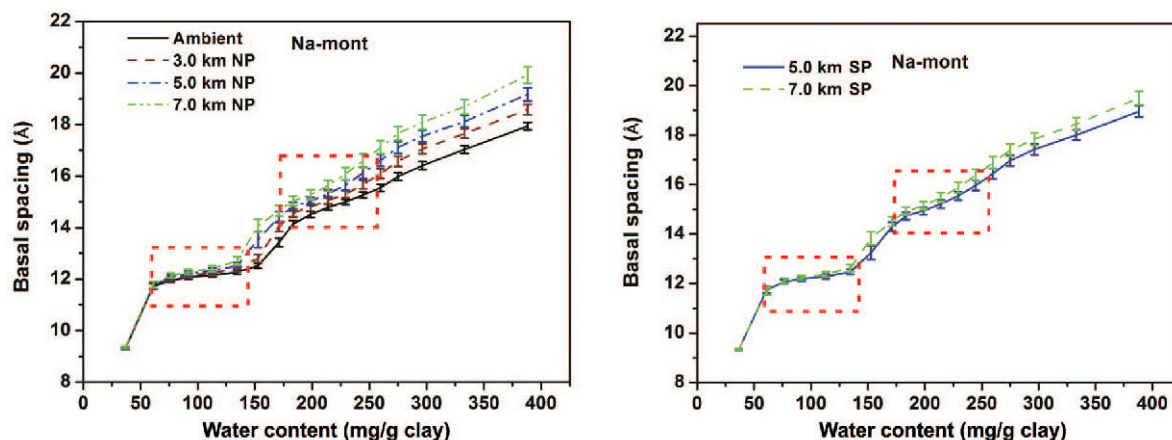
Figure 1. Swelling curves of Na-montmorillonite under: (a) hydrostatic fluid pressure (NP); and (b) lithostatic pressure (SP), at various depths. The first and second plateaus are shown in the dotted boxes.

The basal spacing values for the monolayer and bilayer hydrates under ambient conditions are 12.3 Å and 15.5 Å, respectively. This is consistent with previous studies (Cases *et al.*, 1992; Berend *et al.*, 1995; Laird, 1999; Xu *et al.*, 2000; Hensen *et al.*, 2002). Under NP, the basal spacing range of the bilayer hydrates at 0 km depth (ambient) was ~14.5−15.5 Å, and increased to ~14.8−16.0 Å at a depth of 3.0 km, 14.9−15.7 Å at 5.0 km, and 15.3−16.5 Å at 7.0 km. In SP states, the basal spacing range of the bilayer hydrates at a depth of 5.0 km was 15.0 to 16.0 Å; at 7.0 km depth it was 15.2−16.4 Å. The basal spacing of stable monolayer and bilayer hydrates were determined accurately by integrating both the swelling curves and the immersion energy curves. The basal spacings of stable monolayer and bilayer hydrates under NP and SP are listed in Table 2.

According to the immersion energy curves (Figure 2), the bilayer hydrate seemed more stable than monolayer hydrates under NP from 0 to 7.0 km and under SP at 5 km. Under lithostatic pressure, the monolayer hydrate appears more stable than the bilayer hydrate when the depth increases to 7 km. For clays buried deeply enough, the stable hydrate state would change to the monolayer hydrate. The temperature and pressure of a stable monolayer hydrate of Na-montmorillonite should be greater than that of 7 km under SP. In addition, the simultaneous temperature and pressure changes influenced the water contents of the stable monolayer hydrates and bilayer hydrates. The minima of immersion energy curves at deeper depths appeared at a slightly smaller water content than those at shallower depths. This observation suggests that when the burial depth of hydrated clays increased, some interlayer water would be released into pore spaces.

Density distributions of interlayer species

The water contents of monolayer hydrates and bilayer hydrates were determined based on the minima of immersion energy curves (Figure 2) and the density distribution profiles of the interlayer species were calculated from the NVT simulations shown in Figures 3 and 4. The distributions of water and Na⁺ ions in monolayer hydrates at various depths were exactly the same. In the monolayer hydrate, water molecules were distributed in the medium of the interlayer space and Na⁺ ions were located close to clay surfaces. The increased temperature and pressure hardly influenced the configuration of monolayer hydrate structures. In the bilayer structures under NP, the two clearly separated double peaks of interlayer water broadened gradually and decreased as the burial depth increased. The water peaks under SP show similar

Table 2. Calculated basal spacing and corresponding water content of monolayer and bilayer hydrates at different depths.

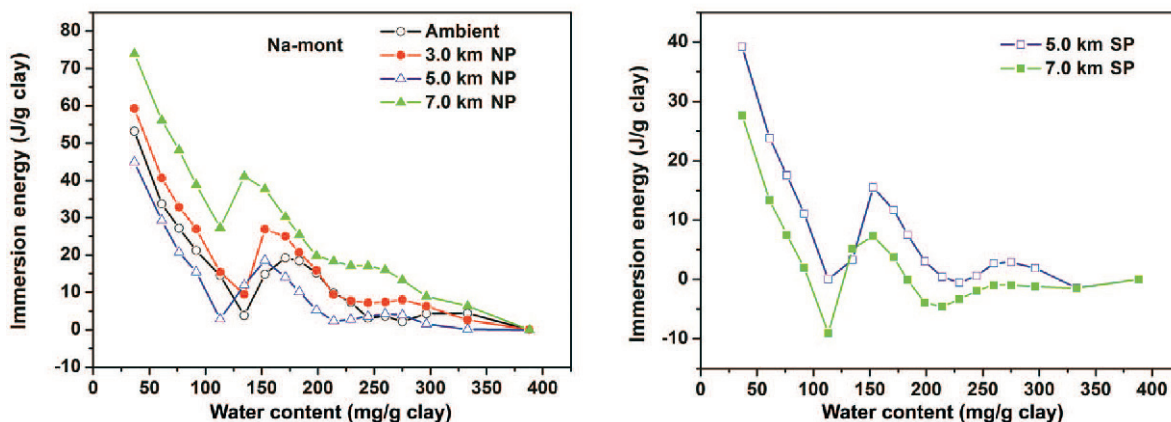| Notation	Basal spacing of stable monolayer hydrate (Å)	Water content of stable monolayer hydrate (mg/g of clay)	Basal spacing of stable bilayer hydrate (Å)	Water content of stable bilayer hydrate (mg/g of clay)
Ambient	12.51	135	15.55	245
3.0 km NP	12.80	135	16.10	245
5.0 km NP	12.52	113	15.65	214
5.0 km SP	12.47	113	15.96	229
7.0 km NP	12.70	113	16.59	229
7.0 km SP	12.62	113	15.88	214

Figure 2. Immersion energy curves of the Na-montmorillonite under: (a) hydrostatic fluid pressure (NP); and (b) lithostatic pressure (SP) at various depths.

changes but to a lesser extent. Interlayer Na$^+$ ions show a three-peaked distribution in bilayer hydrates, with the middle Na$^+$ peak being much greater than the other two side peaks, indicating Na$^+$ ions hopping on clay surfaces. As the burial depth increased, the middle Na$^+$ peak was reduced and broadened while the side peaks increased slightly, eventually turning into three equally high peaks upon reaching 7.0 km under NP. The changes observed

for the middle Na$^+$ peaks under SP were smaller than those under NP.

Mobility of interlayer species

The mobility of interlayer species was evaluated by calculating their diffusion coefficients (Figure 5). Similar to the Na-montmorillonite under ambient conditions, the diffusion coefficient of water was greater
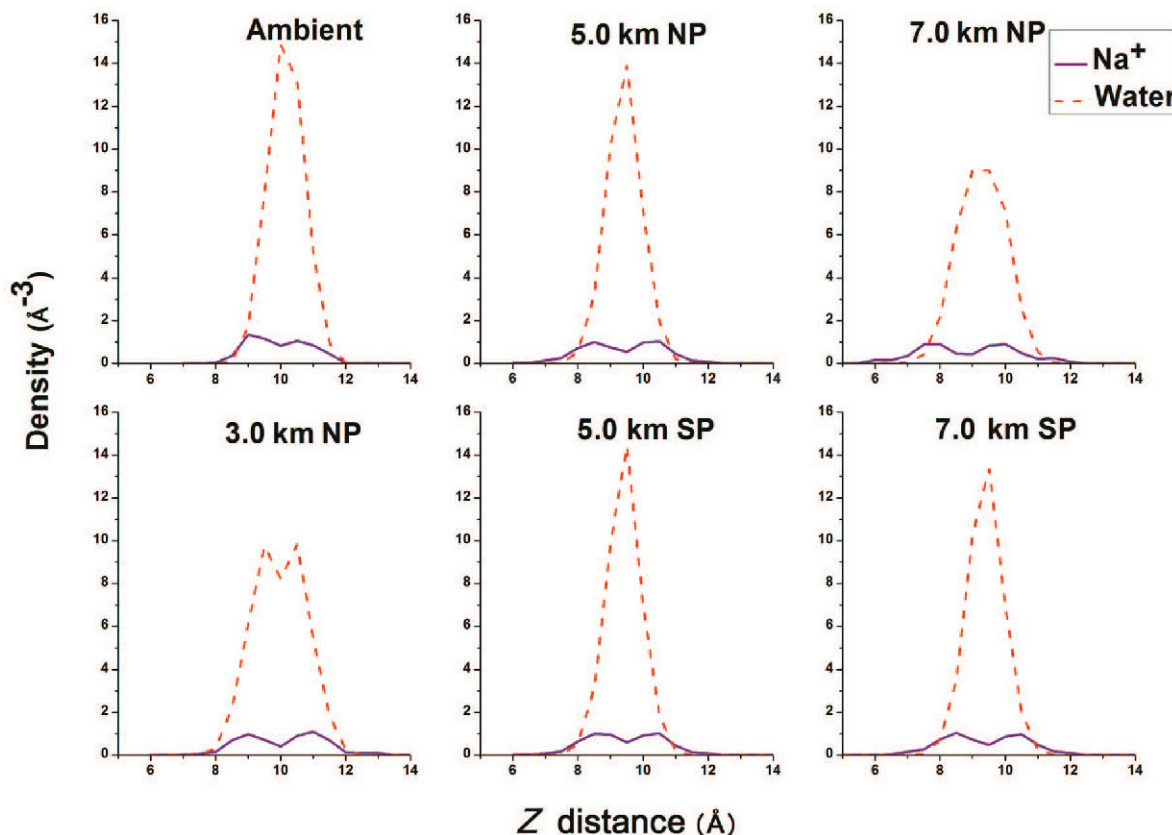

Figure 3. Density distribution profiles of interlayer species in monolayer hydrates of Na-montmorillonite at various depths.
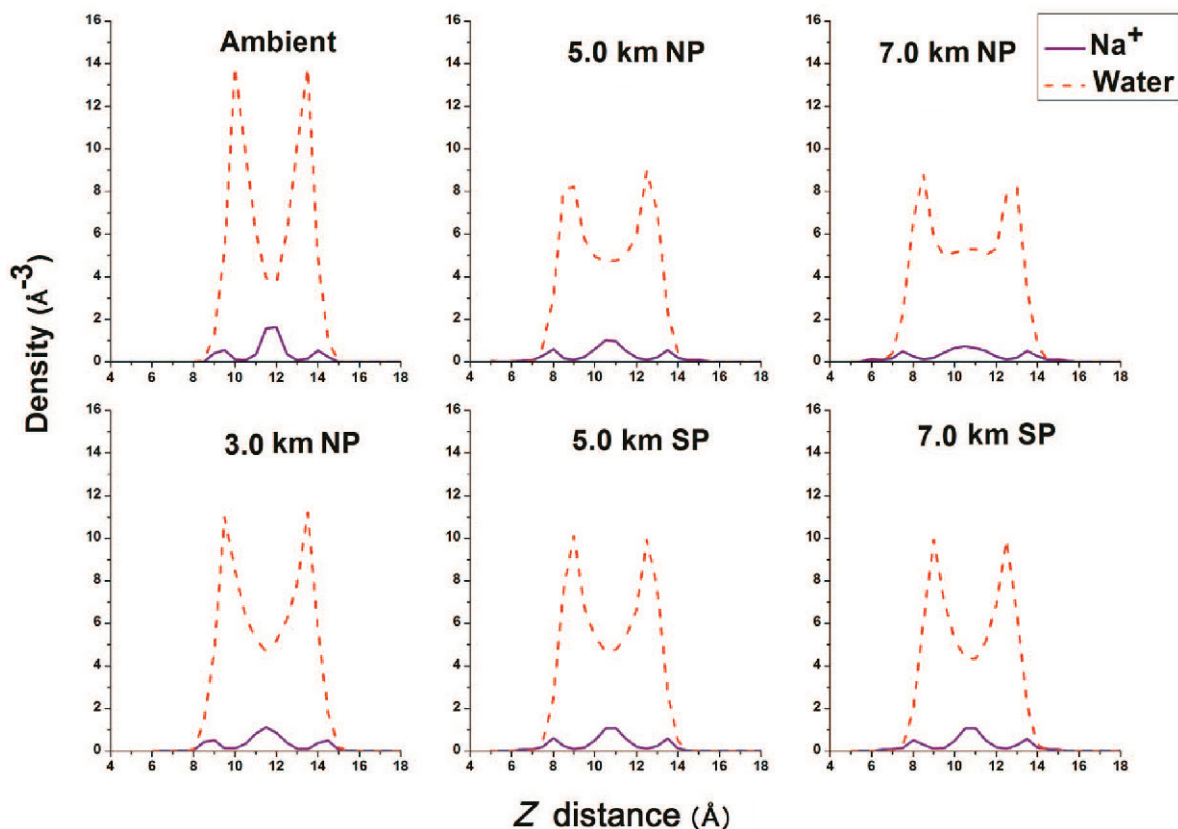
Figure 4. Density distribution profiles of interlayer species in bilayer hydrates of Na-montmorillonite at various depths.

than that of Na^+ ions, as observed previously (Bourg and Sposito, 2010; Zheng and Zaoui, 2013; Holmboe and Bourg, 2014; Zhang *et al.*, 2014), and both values tended to increase with increasing water content. The diffusion coefficients of both water and Na^+ ions in monolayer hydrate or bilayer hydrate under NP were larger than those in monolayer hydrate or bilayer hydrate at the same depth under SP conditions (Figure 5). The differences in diffusion coefficients between water and Na^+ were more obvious in bilayer hydrates than that in
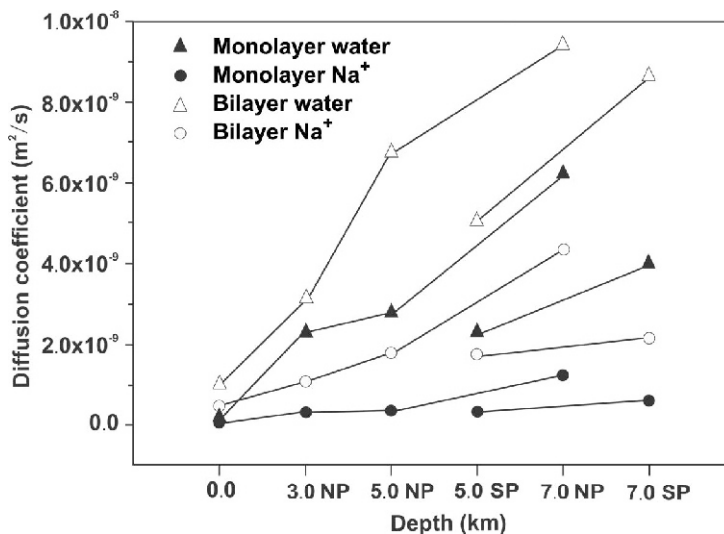

Figure 5. Diffusion coefficients of interlayer water and Na^+ ions in Na-montmorillonite at various depths.

monolayer hydrates. The diffusion coefficients of water and Na^+ ions increased with increasing depth irrespective of whether they were monolayer hydrates or bilayer hydrates under NP or SP states.

DISCUSSION

Coupling effects of temperature and pressure

The transition of stable hydrates (from bilayer to monolayer hydrate) of montmorillonite and the interlayer structures of water and Na^+ ions in montmorillonite can be attributed to the coupled effects of high temperature and high pressure under basin conditions. The basal spacing is sensitive to the temperature and tends to increase when the temperature increases under fixed water content and pressure conditions (Teich-McGoldrick et al., 2015). With simultaneous increase of temperature and pressure, the present results show that the basal spacing of monolayer hydrates at different depths remains at ~12.5 Å (Table 2) and this is consistent with results from a previous study on Na-montmorillonite under basin conditions with different models and force fields (Odriozola and Guevara-Rodríguez, 2004). The basal spacing of the bilayer hydrate at various depths is ~16 Å (Table 2). This is slightly larger than the spacing under ambient conditions. Also notable was the fact that the water content of the stable monolayer and bilayer hydrates decreased gradually with increasing depth.

The stable hydrate structure of Na-montmorillonite under ambient conditions is a bilayer hydrate structure which is generally accepted (Cygan et al., 2009; Anderson et al., 2010). At sufficiently great depths or sufficiently high pressures the stable hydrate structure is no longer the bilayer hydrate but rather the monolayer hydrate. The transition between these two hydrates occurs at temperatures and pressures of ~7.0 km SP, which is quite different from transition depths that were previously determined experimentally (Huang et al., 1994; Wu et al., 1997; De Siqueira et al., 1999). This difference is probably caused by the kinetic constraints of the in situ experiments, in which each interval of temperature and pressure increase took only ~15 min due to the limitation of the finite power of the heaters and the thermal conductivity of the Ti/Zr alloy (De Siqueira et al., 1999). Although those researchers performed at least two runs for each process and acquired similar results, verifying results for conditions approaching equilibrium was difficult because most kinetic processes could be reproduced without reaching a state of equilibrium.

The increments of temperature and pressure used barely influence the configurations of monolayer hydrates. The coupled effects of temperature and pressure on the structure of bilayer hydrates are clearly evident, however (Figure 4). For the systems under NP the water peaks in the density distribution curves broaden with increasing depth. This can be attributed to the slight expansion of the interlayer region. Under SP, the distribution curves of water at depths of 5.0 and 7.0 km are similar. Because the water content of the bilayer hydrate was lower at 7.0 km than at 5.0 km, decreasing the water content neutralized the influence of increasing basal spacing due to depth on the distribution of water and Na^+ ions. Meanwhile, under basin conditions (NP or SP), more Na^+ ions are distributed closer to the clay surface compared to their distribution under ambient conditions, perhaps because high temperature commonly decreases the hydration preference of Na^+ ions as it becomes an entropically unfavorable process (Osakai et al., 2003).

Geological implications

Within sedimentary basins the structural transition from a bilayer hydrate to a monolayer hydrate of montmorillonite or smectite layers in mixed clays due to increasing burial depth implies a natural dehydration event. The weak shrinking of the basal spacing of the bilayer hydrate leads to decreasing water content as its burial depth increases, causing a weak but continuous dehydration process. The release of water into pore spaces is a general process as the basin subsides due to the continuous dehydration of swelling clays. The water expelled from the clay interlayer into the pore spaces will influence the pressure and salinity of the pore fluids directly and contribute further to chemical diagenesis or mechanical rupturing of the host rocks. In addition, the decreasing pore pressure of shale, due generally to drilling or sudden rock rupture, could induce clay swelling and lead to a great reduction in rock strength. This phenomenon should be considered when drilling in a basin or in order to characterize the earthquake evolution (Vrolijk, 1990).

CONCLUSIONS

In the present study, MD simulations were carried out to study systematically the effects of basin conditions on the hydration of Na-montmorillonite under hydrostatic and lithostatic pressures.

With increasing temperature and pressure the basal spacing of Na-montmorillonite varies slightly in monolayer structures and more significantly in bilayer structures. Unlike ambient conditions, the monolayer hydrate structure was found to be more stable than the bilayer hydrate structure at a depth of 7.0 km under lithostatic pressure. The temperature and pressure at 7.0 km were near the transition point for stable hydrate states.

For monolayer-hydrate structures the changes in temperature and pressure have a scarcely noticeable impact on the configurations. In bilayer-hydrate structures the high temperature changed the basal spacing and the distribution preference of Na^+ ions. Under hydro-

static pressure the configurations of bilayer hydrates at greater depths were obviously compressed compared to their configurations under ambient conditions. Under lithostatic pressure, sufficiently high pressure could be achieved to decrease or neutralize part of the impact of the high temperature on the configurations of bilayer hydrates. Similarly the high pressure counteracted some of the influence of high temperature on the dynamics of the interlayer species. Under hydrostatic pressure, the mobility of interlayer water and ions clearly increased due to the increment of temperature. Comparing the mobility at the same depths under hydrostatic pressure and lithostatic pressure, the increased pressure decreased the mobility of interlayer water and ions.

ACKNOWLEDGMENTS

REFERENCES

Anderson, R., Ratcliffe, I., Greenwell, H., Williams, P., Cliffe, S., and Coveney, P. (2010) Clay swelling − a challenge in the oilfield. *Earth-Science Reviews*, **98**, 201−216.

Berend, I., Cases, J.M., Francois, M., Uriot, J.P., Michot, L., Masion, A., and Thomas, F. (1995) Mechanism of adsorption and desorption of water-vapor by homoionic montmorillonites. 2. The Li^+, Na^+, K^+, Rb^+ and Cs^+-exchanged forms. *Clays and Clay Minerals*, **43**, 324−336.

Boek, E.S. and Sprik, M. (2003) Ab initio molecular dynamics study of the hydration of a sodium smectite clay. *Journal of Physical Chemistry B*, **107**, 3251−3256.

Boek, E.S., Coveney, P.V., and Skipper, N.T. (1995a) Molecular modeling of clay hydration: A study of hysteresis loops in the swelling curves of sodium montmorillonites. *Langmuir*, **11**, 4629−4631.

Boek, E.S., Coveney, P.V., and Skipper, N.T. (1995b) Monte Carlo molecular modeling studies of hydrated Li-, Na-, and K-smectites: Understanding the role of potassium as a clay swelling inhibitor. *Journal of the American Chemical Society*, **117**, 12608−12617.

Bourg, I.C. and Sposito, G. (2010) Connecting the molecular scale to the continuum scale for diffusion processes in smectite-rich porous media. *Environmental Science & Technology*, **44**, 2085−2091.

Brown, G. and Brindley, G.W. (1980) *Crystal Structures of Clay Minerals and their X-ray Identification*. Monograph **5**, Mineralogical Society of Great Britian & Ireland.

Cases, J.M., Berend, I., Besson, G., Francois, M., Uriot, J.P., Thomas, F., and Poirier, J.E. (1992) Mechanism of adsorption and desorption of water-vapor by homoionic montmorillonite. 1. The sodium-exchanged form. *Langmuir*, **8**, 2730−2739.

Cases, J.M., Berend, I., Francois, M., Uriot, J.P., Michot, L.J., and Thomas, F. (1997) Mechanism of adsorption and desorption of water vapor by homoionic montmorillonite. 3. The Mg^{2+}, Ca^{2+}, Sr^{2+} and Ba^{2+} exchanged forms. *Clays and Clay Minerals*, **45**, 8−22.

Cygan, R.T., Liang, J.-J., and Kalinichev, A.G. (2004) Molecular models of hydroxide, oxyhydroxide, and clay phases and the development of a general force field. *The Journal of Physical Chemistry B*, **108**, 1255−1266.

Cygan, R.T., Greathouse, J.A., Heinz, H., and Kalinichev, A.G. (2009) Molecular models and simulations of layered materials. *Journal of Materials Chemistry*, **19**, 2470−2481.

Dazas, B., Ferrage, E., Delville, A., and Lanson, B. (2014) Interlayer structure model of tri-hydrated low-charge smectite by X-ray diffraction and Monte Carlo modeling in the Grand Canonical ensemble. *American Mineralogist*, **99**, 1724−1735.

De Pablo, L., Chavez, M.L., and De Pablo, J.J. (2005) Stability of Na-, K-, and Ca-montmorillonite at high temperatures and pressures: A Monte Carlo simulation. *Langmuir*, **21**, 10874−10884.

De Siqueira, A.V.C., Skipper, N.T., Coveney, P.V., and Boek, E.S. (1997) Computer simulation evidence for enthalpy driven dehydration of smectite clays at elevated pressures and temperatures. *Molecular Physics*, **92**, 1−6.

De Siqueira, A.V., Lobban, C., Skipper, N.T., Williams, G.D., Soper, A.K., Done, R., Dreyer, J.W., Humphreys, R.J., and Bones, J.A. (1999) The structure of pore fluids in swelling clays at elevated pressures and temperatures. *Journal of Physics: Condensed Matter*, **11**, 9179.

Deming, D. (2002) *Introduction to Hydrogeology*. McGraw-Hill, New York.

Ferrage, E., Lanson, B., Malikova, N., Plançon, A., Sakharov, B.A., and Drits, V.A. (2005a) New insights on the distribution of interlayer water in bi-hydrated smectite from X-ray diffraction profile modeling of 00l reflections. *Chemistry of Materials*, **17**, 3499−3512.

Ferrage, E., Lanson, B., Sakharov, B.A., and Drits, V.A. (2005b) Investigation of smectite hydration properties by modeling experimental X-ray diffraction patterns: Part I. montmorillonite hydration properties. *American Mineralogist*, **90**, 1358−1374.

Ferrage, E., Lanson, B., Michot, L.J., and Robert, J.-L. (2010) Hydration properties and interlayer organization of water and ions in synthetic Na-smectite with tetrahedral layer charge. Part 1. Results from X-ray diffraction profile modeling. *Journal of Physical Chemistry C*, **114**, 4515−4526.

Greathouse, J.A., Stellalevinsohn, H.R., Denecke, M.A., Bauer, A., and Pabalan, R.T. (2005) Uranyl surface complexes in a mixed-charge montmorillonite: Monte Carlo computer simulation and polarized XAFS results. *Clays and Clay Minerals*, **53**, 278−286.

Guggenheim, S. and Van Groos, A.K. (2001) Baseline studies of The Clay Minerals Society source clays: thermal analysis. *Clays and Clay Minerals*, **49**, 433−443.

Heinz, H., Koerner, H., Anderson, K.L., Vaia, R.A., and Farmer, B. (2005) Force field for mica-type silicates and dynamics of octadecylammonium chains grafted to montmorillonite. *Chemistry of Materials*, **17**, 5658−5669.

Hensen, E.J. and Smit, B. (2002) Why clays swell? *The Journal of Physical Chemistry B*, **106**, 12664−12667.

Holmboe, M. and Bourg, I.C. (2014) Molecular dynamics simulations of water and sodium diffusion in smectite interlayer nanopores as a function of pore size and temperature. *The Journal of Physical Chemistry C*, **118**, 1001−1013.

Holmboe, M., Wold, S., and Jonsson, M. (2012) Porosity investigation of compacted bentonite using XRD profile modeling. *Journal of Contaminant Hydrology*, **128**, 19−32.

Huang, W.L., Bassett, W.A., and Wu, T.C. (1994) Dehydration and hydration of montmorillonite at elevated temperatures and pressures monitored using synchrotron radiation. *American Mineralogist*, **79**, 683−691.

Hunt, J.M. (1990) Generation and migration of petroleum from abnormally pressured fluid compartments. *AAPG Bulletin*, **74**, 1−12.

Kim, N., Kim, Y., Tsotsis, T.T., and Sahimi, M. (2005) Atomistic simulation of nanoporous layered double hydroxide materials and their properties. I. Structural modeling. *Journal of Chemical Physics*, **122**.

Kumar, P.P., Kalinichev, A.G., and Kirkpatrick, R.J. (2007) Molecular dynamics simulation of the energetics and structure of layered double hydroxides intercalated with carboxylic acids. *Journal of Physical Chemistry C*, **111**, 13517−13523.

Laird, D.A. (1999) Layer charge influences on the hydration of expandable 2:1 phyllosilicates. *Clays and Clay Minerals*, **47**, 630−636.

Liu, X.D. and Lu, X.C. (2006) A thermodynamic understanding of clay-swelling inhibition by potassium ions. *Angewandte Chemie, International Edition*, **45**, 6300−6303.

Liu, X.D., Lu, X.C., Wang, R.C., and Zhou, H.Q. (2008) Effects of layer-charge distribution on the thermodynamic and microscopic properties of Cs-smectite. *Geochimica et Cosmochimica Acta*, **72**, 1837−1847.

Loewenstein, W. (1954) The distribution of aluminum in the tetrahedra of silicates and aluminates. *American Mineralogist*, **39**, 92−96.

Meunier, A. (2005) *Clays*. Springer Science & Business Media.

Odriozola, G. and Guevara-Rodríguez, F.d.J. (2004) Na-montmorillonite hydrates under basin conditions: Hybrid Monte Carlo and molecular dynamics simulations. *Langmuir*, **20**, 2010−2016.

Osakai, T., Tokura, A., Ogawa, H., Hotta, H., Kawakami, M. and Akasaka, K. (2003) Temperature effect on the selective hydration of sodium ion in nitrobenzene. *Analytical Sciences*, **19**, 1375−1380.

Petit, S. and Madejová, J. (2013) Fourier transform infrared spectroscopy. Pp. 213−231 in: *Handbook of Clay Science*, 2nd edition (F. Bergaya and G. Lagaly, editors). Developments in Clay Science, **5**, Elsevier, Amsterdam.

Plimpton, S. (1995) Fast parallel algorithms for short-range molecular dynamics. *Journal of Computational Physics*, **117**, 1−19.

Rick, S.W., Stuart, S.J., and Berne, B.J. (1994) Dynamical fluctuating charge force-fields − application to liquid water. *Journal of Chemical Physics*, **101**, 6141−6156.

Shahriyari, R., Khosravi, A., and Ahmadzadeh, A. (2013) Nanoscale simulation of Na-montmorillonite hydrate under basin conditions, application of CLAYFF force field in parallel GCMC. *Molecular Physics*, **111**, 3156−3167.

Smith, D.E. (1998) Molecular computer simulations of the swelling properties and interlayer structure of cesium montmorillonite. *Langmuir*, **14**, 5959−5967.

Smith, D.E., Wang, Y., Chaturvedi, A., and Whitley, H.D. (2006) Molecular simulations of the pressure, temperature, and chemical potential dependencies of clay swelling. *The Journal of Physical Chemistry B*, **110**, 20046−20054.

Tambach, T.J., Hensen, E.J., and Smit, B. (2004) Molecular simulations of swelling clay minerals. *The Journal of Physical Chemistry B*, **108**, 7586−7596.

Teich-McGoldrick, S.L., Greathouse, J.A., Jové-Colón, C.F., and Cygan, R.T. (2015) Swelling properties of montmorillonite and beidellite clay minerals from molecular simulation: comparison of temperature, interlayer cation, and charge location effects. *The Journal of Physical Chemistry C*, **119**, 20880−20891.

Teppen, B.J., Rasmussen, K., Bertsch, P.M., Miller, D.M., and Schäfer, L. (1997) Molecular dynamics modeling of clay minerals. 1. Gibbsite, kaolinite, pyrophyllite, and beidellite. *The Journal of Physical Chemistry B*, **101**, 1579−1587.

Wang, J., Kalinichev, A.G., and Kirkpatrick, R.J. (2006) Effects of substrate structure and composition on the structure, dynamics, and energetics of water at mineral surfaces: A molecular dynamics modeling study. *Geochimica et Cosmochimica Acta*, **70**, 562−582.

Wang, J.W., Kalinichev, A.G., and Kirkpatrick, R.J. (2004) Molecular modeling of water structure in nano-pores between brucite (001) surfaces. *Geochimica et Cosmochimica Acta*, **68**, 3351−3365.

Wu, T.C., Bassett, W.A., Huang, W.L., Guggenheim, S., and Koster van Groos, A.F. (1997) Montmorillonite under high H_2O pressures: Stability of hydrate phases, rehydration hysteresis, and the effect of interlayer cations. *American Mineralogist*, **82**, 69−78.

Xie, X., Bethke, C.M., Li, S., Liu, X., and Zheng, H. (2001) Overpressure and petroleum generation and accumulation in the Dongying Depression of the Bohaiwan Basin, China. *Geofluids*, **1**, 257−271.

Xu, W.Z., Johnston, C.T., Parker, P., and Agnew, S.F. (2000) Infrared study of water sorption on Na-, Li-, Ca-, and Mg-exchanged (SWy-1 and SAz-1) montmorillonite. *Clays and Clay Minerals*, **48**, 120−131.

Zhang, L.H., Lu, X.C., Liu, X.D., Zhou, J.H., and Zhou, H.Q. (2014) Hydration and mobility of interlayer ions of (Na_x, Ca_y)-montmorillonite: A molecular dynamics study. *The Journal of Physical Chemistry C*, **118**, 29811−29821.

Zheng, Y. and Zaoui, A. (2013) Temperature effects on the diffusion of water and monovalent counterions in the hydrated montmorillonite. *Physica A: Statistical Mechanics and Its Applications*, **392**, 5994−6001.